Selenium-Modified Titanium Dioxide Photochemical Diode/Electrolyte Junctions: Photocatalytic and Electrochemical Preparation, Characterization, and Model Simulations

Norma R. de Tacconi,* C. R. Chenthamarakshan, and Krishnan Rajeshwar*

Department of Chemistry and Biochemistry, The University of Texas at Arlington, Arlington, Texas 76019-0065

Eugenio J. Tacconi

Megger Engineering Group, Dallas, Texas 75237-1019

Received: December 22, 2004; In Final Form: April 25, 2005

The photoelectrochemical behavior of TiO_2 thin film electrodes, photocatalytically modified with Se islands, is described. The TiO_2 thin films were electrodeposited on transparent conducting oxide glass substrates. The resultant electrode forms a n-TiO_2/p-Se "photochemical diode" which, in turn, contacts an electrolyte phase. Both transient photocurrent profiles (in response to excitation light that is switched on or off) and steady-state current−potential curves in response to chopped irradiation are considered. We show that the relative dominance of the contributions from the TiO_2 and Se components to the overall response of the photochemical diode/electrolyte junction crucially depends on the wavelength distribution of the excitation light source. A simple equivalent circuit representation of this junction is presented, comprised of a photodiode in parallel with two photodiodes connected in series back-to-back. Simulations of the transient and steady-state photoelectrochemical response of this system are presented, and are shown to be in good agreement with the corresponding experimental profiles.

Introduction

Novel configurations for semiconductor−electrolyte junctions have relevance to a variety of practical applications ranging from solar energy conversion to chemical sensors. Several types of such monolithic structures have been reviewed.[1] Perhaps the simplest is the Schottky barrier[2] type of structure resulting from platinization of a semiconductor surface and its subsequent immersion and use in a liquid electrolyte (see, for example, Figure 12 in ref 1). Alternately, a n-type semiconductor can be mated with a p-type semiconductor to afford a "photochemical diode".[1,3] Even two different (particulate) semiconductors of the same type (say, n) can be combined in a composite configuration.[4] Finally, an integrated, monolithic electrode design comprised of a p−n photovoltaic junction biasing a p-type semiconductor (e.g., p-$GaInP_2$) has been deployed for photoelectrolyzing water.[5]

In previous papers from this laboratory,[6,7] we showed how photocatalysis could be used for preparing n-TiO_2/p-Se diodes. A similar approach was also used by another group, who discussed the interesting properties of this diode in contact with an electrolyte junction under UV illumination.[8] In the present paper, we further elaborate on the photoelectrochemical properties of this diode in contact with an inert supporting electrolyte at fixed potentials (photocurrent−time transient profiles) and under potentiodynamic (swept potential) conditions. We show that the relative dominance of the contributions from the TiO_2 and Se components to the overall photoelectrochemical behavior of the diode crucially depends on the wavelength distribution of the excitation light source employed. Finally, both the measured transient profiles and the potentiodynamic photoelec-

trochemical behavior of the n-TiO_2/p-Se/electrolyte junction are simulated by a simple equivalent circuit model.

Experimental Section

Chemicals and Materials. All chemicals were from commercial sources and were the highest purity available. [Caution: Selenium solutions are toxic; their handling and disposal must be done with extreme care.] Deionized water (18 MΩ) was used in all cases for making solutions. Either polycrystalline gold or transparent conducting oxide (TCO) was used as the substrate for the working electrode films. The latter consisted of F-doped tin oxide (Nippon Sheet Glass Ltd.) coated on soda-lime glass. They were nominally ca. 400 nm thick and had a sheet resistance of 10.3 Ω/□. Strips (0.65 × 2 cm²) were cut and cleaned in four 5 min steps of cleansing in ultrasonicated acetone, ethanol, 1:1 H_2O_2/ammonia, and finally ultrapure water. The Au disk electrodes (Bioanalytical Systems, 0.018 cm² geometric area) were mechanically polished to mirror finish using alumina particles (Buehler) of successively finer size (1.0 μm, 0.3 μm, and 0.05 μm) on a microcloth (Buehler No. 40-7212). They were then ultrasonically cleaned in water for 1 min.

Electrosynthesis. Titanium dioxide films were cathodically electrosynthesized on TCO substrates from a peroxotitanium precursor bath containing nitrate ions.[9] The bath preparation has been described by other authors[9] but briefly consists of dissolving Ti powder in a solution containing H_2O_2 and NH_3. The gel initially formed is redissolved in HNO_3. The pH of this solution is then adjusted to 1.7 with dilute NH_3. Film formation occurs in this process by the initial electrogeneration of base and an increase in the local pH at the substrate/solution interface.[10,11] The titanium hydroxide gel film was obtained on the substrate by reaction of the electrogenerated base with the Ti peroxo species in solution.[12] Thus the titanium precursor

* Authors to whom correspondence should be addressed. E-mail: de Tacconi, ntacconi@uta.edu; Rajeshwar, rajeshwar@uta.edu.

concentration (8−10 mM), bath pH (~1.7), and applied potential (−0.9 to −1.0 V) must be precisely controlled to secure good-quality films. Considerable effort was initially expended to optimize the film deposition variables. The precursor bath was used immediately after preparation as incipient colloid formation occurs in solutions aged for several hours. Both the precursor concentration and medium pH are crucial variables for stabilizing the solutions against fast colloid formation. Nominal deposition periods ranged from 20 to 25 min to afford micrometer-thick films. These oxide films were compact and visually very smooth (see Figure 1, for example). The deposited films were given a thermal anneal of 400 °C for 30 min in all the cases.

For comparison purposes, selenium layers were grown on Au substrates from 10 mM SeO$_2$ in 0.1 M Na$_2$SO$_4$ at a fixed potential of −0.7 V (vs Ag|AgCl|satd. KCl reference; all potentials in this study are quoted with respect to this reference) for 15 min. From the electrodeposition charge an approximate film thickness of 130−180 nm could be estimated for these layers.

Photocatalytic Preparation of n-TiO$_2$/p-Se Diodes. The diodes were prepared according to procedures described by us in previous articles.[6,7] Briefly, the TiO$_2$ film-coated TCO slides were placed in a quartz cell containing an aqueous solution of 0.4 mM SeO$_2$ and irradiated with the full output of a Xe arc lamp (see specifications below) for 2 h. To avoid solution heating, a 2.5 cm water filter (made of two parallel quartz plates) was interposed between the quartz cell and the Xe lamp.

Radiation Sources. A Xe arc lamp and a tungsten (W)-halogen source (with a quartz envelope) were used in this study. Both lamps were operated at full output at their rated 75 and 100 W levels, respectively. For the Xe arc case, the photon flux was ~0.45 mW/cm^2 at 340 nm. The W-halogen lamp had a measured photon flux of ~0.28 mW/cm^2 at 500 nm. The bandwidth in both cases was 4 nm. The Xe lamp was an Oriel Model 66173 operated in conjunction with a power supply (Oriel Model 68806). The W-halogen lamp was operated with an Oriel Model 68735 power supply. The photon fluxes were measured on an Oriel radiant power/energy meter (Model 70260) and the fluxes quoted above are not corrected for reflection losses by cell windows etc.

Electrochemistry/Photoelectrochemistry. A standard single-compartment, three-electrode electrochemical cell was used both for film preparation and for the electrochemical/photoelectrochemical measurements. A large Pt coil and an Ag|AgCl| satd. KCl reference electrode (Microelectrode Inc.), along with the working electrode, completed the cell setup. Electrodeposition was carried out on a Model 100A Electrochemical Analyzer [Bioanalytical Systems (BAS), West Lafayette, IN]. Photovoltammetry and transient photocurrent−time profiles were recorded on a Model CV-27 BAS voltammograph. All the electrolyte solutions (both for film preparation and for the photoelectrochemical measurements) were sparged with ultra-pure N$_2$ for at least 20 min prior to use. All measurements described below were performed at the laboratory ambient temperature (25 ± 2 °C).

Other Instrumentation. For scanning electron microscopy (SEM), a JEOL Model JSM 35C instrument was used, operating at 15 kV. The samples were coated with Au−Pd alloy prior to examination under the microscope. Scanning tunneling microscopy (STM) measurements were made with a Nanoscope E (Digital Instruments, Santa Barbara, CA) Model ECM-NS3 instrument, using Pt/Ir tips (Nanotips; Digital Instruments) that were electrochemically etched in a 20% KCN solution. The tips
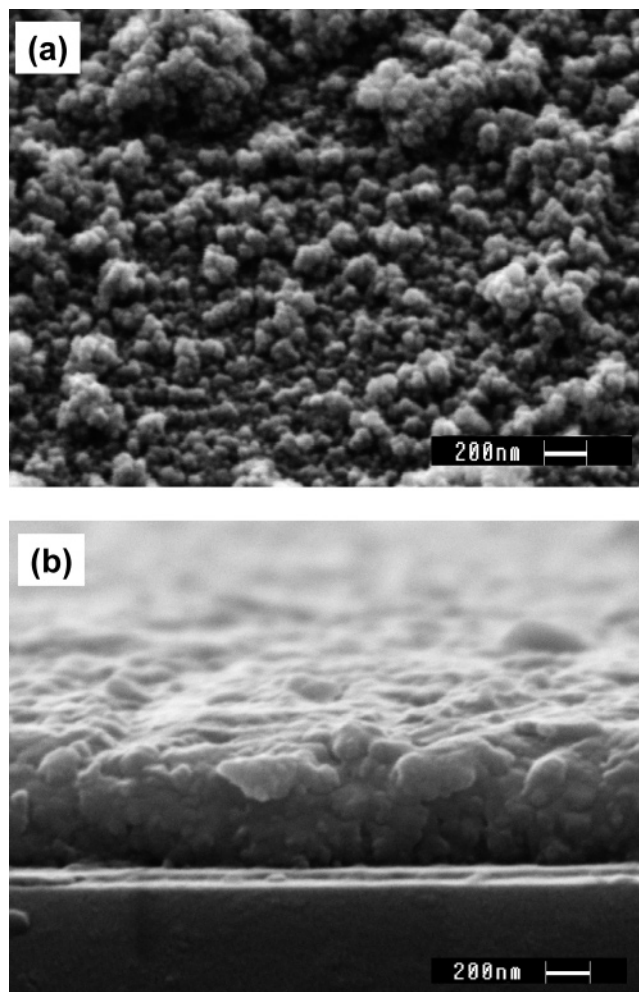

Figure 1. Top view (a) and cross-section (b) by SEM of an electrodeposited TiO$_2$ layer on TCO substrates. The layer was given a thermal anneal (see Experimental Section) prior to SEM examination. Film thickness is ca. 592 nm as provided by the SEM cross-section.

were immersed ~4−5 mm in the etch bath and subjected to 4.8 V AC voltage for 4 min, using a platinum foil as counter electrode. They were then progressively emersed under polarization to concentrate the etch current at the very low end of the tip. The last step improves the tip sharpness significantly, which was verified with an optical microscope. All STM images consist of 256 × 256 data points and were taken in constant height mode. X-ray photoelectron spectroscopy (XPS) used a Perkin-Elmer/Physical Electronics Model 5000C system with details as given elsewhere.[13]

Results and Discussion

Film Morphology and Topography. Figure 1 contains top and cross-sectional views of electrodeposited TiO$_2$ layers as seen by SEM. The film is seen to be quite compact, and the grains are nanometer-sized (see top SEM picture) in agreement with STM data. Representative STM images of the electrodeposited TiO$_2$ film before (Figure 2a) and after (Figure 2b) photocatalytic modification with selenium are contained in Figure 2. Table 1 contains data on the grain height, grain diameter, and grain footprint (base area) computed from these microscopy data for the two types of samples. Importantly, the grain footprint for TiO$_2$/Se films is seen to be smaller than that of the TiO$_2$ host pointing to an island topography for the deposited selenium. Interestingly, this trend coincides with the island growth

Behavior of Se-Modified TiO$_2$ Thin Film Electrodes

J. Phys. Chem. B, Vol. 109, No. 24, 2005 **11955**
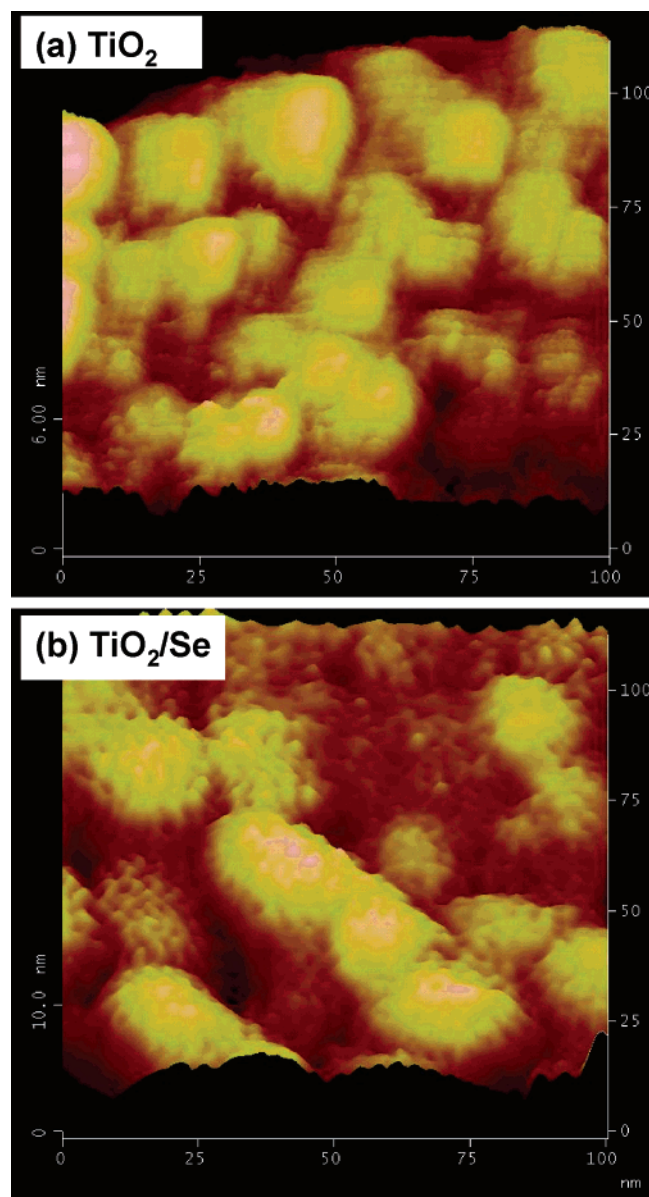
Figure 2. STM images of the electrodeposited TiO$_2$ film before (a) and after (b) photocatalytic modification with selenium. For TiO$_2$ the tip bias (E_{tip}) was 470 mV, the tunneling current (I_t) was 135 pA, and the scan frequency (f) was 3.69 Hz. For TiO$_2$/Se: E_{tip} = −4780 mV, I_t = 496 pA, and f = 5.09 Hz.
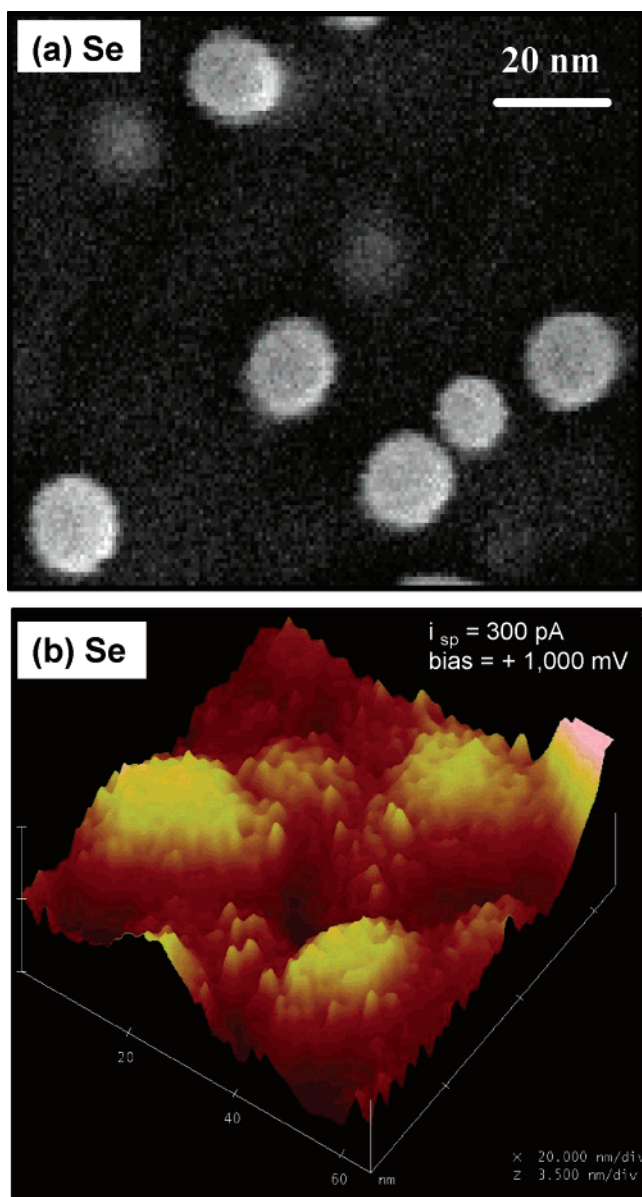

Figure 3. Comparative SEM (a) and STM (b) images of electrodeposited Se film on polycrystalline gold substrate. Films were grown by a potentiodynamic scan between 0 and −0.6 V at 20 mV/s (a) and at a constant potential of −0.7 V (b). Both films were prepared from 10 mM SeO$_2$ + 0.1 M Na$_2$SO$_4$. For the STM image: E_{tip} = 1000 mV, I_t = 300 pA, and f = 10 Hz.

TABLE 1: Morphological Data from Scanning Tunneling Microscopy

sample	grain height (nm)	grain diameter (nm)	grain footprint (nm^2)
TiO$_2^a$	3.8	9.6	72
TiO$_2$/Se^a	2.5	6.5	33
Au/Se	10	17	229

^{a} Film supported by transparent conducting oxide substrate; see the Experimental Section.

behavior of electrosynthesized selenium on gold electrodes (Figure 3) as revealed by both SEM (Figure 3a) and STM (Figure 3b) data. Also included for comparison in Table 1 are the STM-derived grain morphology data for these samples. The discontinuous nature of the Se deposits on the TiO$_2$ surface has important ramifications for device modeling as elaborated later.

Surface Analysis of TiO$_2$/Se Films by XPS. Aside from the expected intense signals from Ti and O (in TiO$_2$), a peak for

Se was clearly seen. The Ti 2p$_{1/2}$ and 2p$_{3/2}$ signals were located at 459.8 and 465.4 eV with a peak separation of 5.6 eV, almost in exact agreement with literature values.[14] The signal for Se 3d at 56.1 eV is to be compared with 55.3 eV reported in the literature.[14] From the high-resolution XPS data, a concentration ratio, Ti:Se, of 89:11 (atom %) could be estimated.

Photoelectrochemical Behavior. Photocurrent/potential profiles under chopped irradiation (0.1 Hz) for the individual components, TiO$_2$ and Se, are presented in Figure 4. The photocurrent profiles for these two components will be useful in the analysis of the behavior of the TiO$_2$/Se bilayer (see below). Both photocurrent−potential curves were taken in the same supporting electrolyte, 0.1 M Na$_2$SO$_4$. The n- and p-type behavior of TiO$_2$ and Se is clearly seen in this comparison, with the photocurrent signals being "up" (anodic) for TiO$_2$ and "down" (cathodic) for Se, respectively. The electrochemical processes contributing to these photocurrents presumably are the oxidation of water (for TiO$_2$) and the reduction of protons
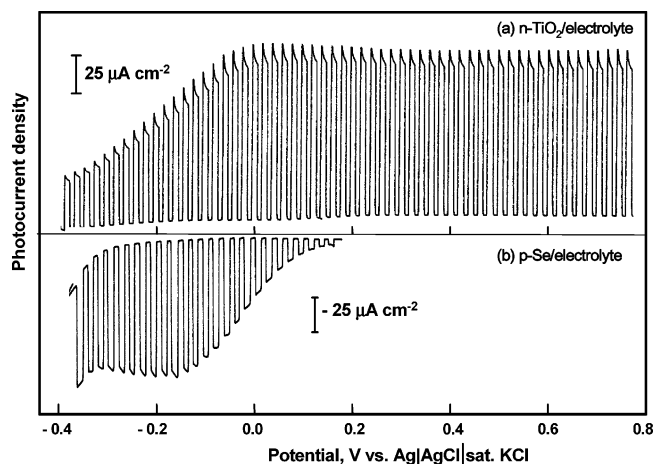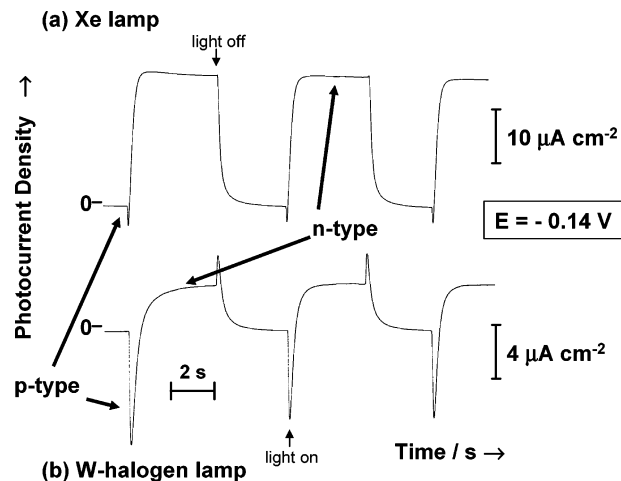
Figure 4. Photocurrent−potential profiles at 0.1 Hz chopped irradiation for electrodeposited TiO_2 (top) and Se (bottom) films in 0.1 M Na_2SO_4. The two films were electrodeposited on TCO and Au substrates, respectively (see the Experimental Section). Photovoltammograms were obtained at 2 mV/s by using the full output of a 75 W Xe lamp. See the Experimental Section for the film electrodeposition conditions.
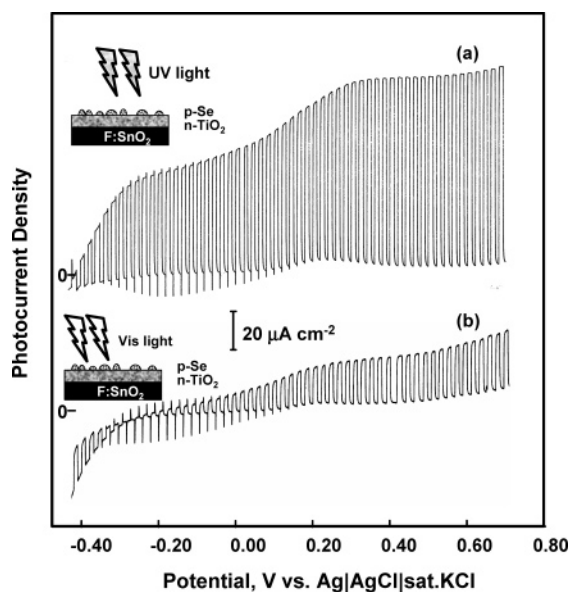

Figure 5. Photocurrent−potential profiles at 0.1 Hz chopped irradiation for n-TiO_2/p-Se/electrolyte junction diodes under irradiation with the Xe arc lamp (a) and with a W-halogen lamp (b). The inserts are schematic sketches of the interface and the type of irradiation used. Other conditions are as in Figure 4.

(for Se) although no attempts were made to analyze for the generated products in the two cases. The photooxidation of water on the TiO_2 surface is a well-established reaction.[1,15,16] For the Se case, other potentially competitive processes to the hydrogen evolution reaction such as the photocorrosion of Se itself can be ruled out on the basis of previous work in the literature.[17]

Figure 5 contains corresponding data for the n-TiO_2/p-Se/electrolyte junction under irradiation with the Xe lamp (Figure 5a) and using a W-halogen lamp (Figure 5b). The effect of the much smaller absorption cross-section of the TiO_2 component with the visible light output of the lamp is clearly seen in two ways: (a) The photoanodic output in the range of potentials from −0.40 to ~0 V is almost nonexistent in Figure 5b relative to Figure 5a. (b) The S-shaped photoanodic envelope (that is a signature for n-type semiconductor/electrolyte junction, refs 18 and 19) at potentials more positive than 0 V is drastically diminished in Figure 5b relative to Figure 5a.
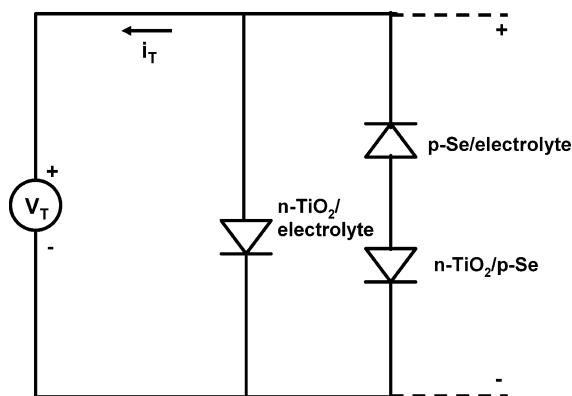

Figure 6. Comparison of the effect of excitation wavelengths on the photoresponse of the n-TiO_2/p-Se/electrolyte junction as provided by transient photocurrent profiles: (a) Xe lamp and (b) W-halogen lamp.
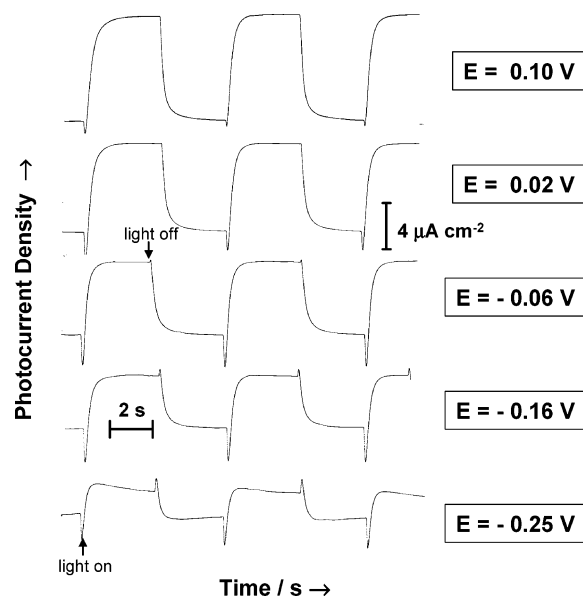
Figure 7. Effect of bias potential on the transient photoresponse for the n-TiO_2/p-Se/electrolyte junction in 0.1 M Na_2SO_4 under Xe arc lamp irradiation.

Further insights into the effect of excitation wavelengths on the photoresponse of the n-TiO_2/p-Se/electrolyte junction are provided by the transient photocurrent profiles in Figure 6. In Figure 6a for Xe arc lamp irradiation, the dominant photoanodic response is from the TiO_2 component and only a trace of the faster photocathodic (spiked) response, attributable to the Se component, is seen. On the other hand, this faster photocathodic spike is much more prominent under W-halogen excitation (Figure 6b). The two sets of data in Figure 6 were obtained at a fixed potential of −0.14 V.

The effect of polarization potential (of the n-TiO_2/p-Se/electrolyte junction) on the transient photoresponse is brought out by the data contained in Figure 7 with Xe arc irradiation. Clearly, the net influence of the two variables (excitation wavelength and polarization potential) on the photoresponse is not dissimilar (cf., Figures 6 and 7). A systematically more negative bias potential (driving the electrons to the electrolyte side of the junction) (Figure 7) provokes a very similar type of photoresponse to exciting dominantly the p-Se side of the n-TiO_2/p-Se/electrolyte junction.

Behavior of Se-Modified TiO₂ Thin Film Electrodes

J. Phys. Chem. B, Vol. 109, No. 24, 2005 **11957**

Figure 8. Equivalent circuit representation of the n-TiO₂/p-Se/electrolyte junction. V_T is the total applied bias and i_T is the total photocurrent containing contributions from the two parallel circuit branches.

Model Simulations. A very simple equivalent circuit model consisting of photodiodes in series and parallel was used to simulate the measured transient photoresponse profiles (Figures 6 and 7). Since the TiO₂ surface is not completely covered by Se (cf., Figures 2 and 3, and XPS assay), allowance must be made for a parallel photocurrent flow pathway across the bare TiO₂/electrolyte interfaces. This is done in the simple equivalent circuit representation of the n-TiO₂/p-Se/electrolyte junction in Figure 8. The following equations were used for simulating the transient photocurrent profiles in Figures 6 and 7:

$$j_{ph} = a_1[1 - e^{-b_1 t}] - a_2[1 - e^{-b_2 t}] \qquad (1)$$

$$j_d = a_1'[1 - e^{-b_1 t}] - a_2'[1 - e^{-b_2 t}] \qquad (2)$$

In eqs 1 and 2, j_{ph} is the photocurrent density ($j_{ph} = i_{ph}/A$, where A is the geometric photoelectrode area) and j_d is the corresponding dark current density. The first terms in eqs 1 and 2 represent the contribution from the bare TiO₂/electrolyte contacts and the second terms account for the parallel photodiode-in-series branch representing the n-TiO₂/p-Se/electrolyte junction (Figure 8). The opposite signs for the two terms in eqs 1 and 2 are consistent with the fact that a n-type semiconductor (TiO₂) contacts the electrolyte in the first branch while a p-type semiconductor (Se) contacts the electrolyte in the second (parallel) branch of the overall circuit. The dominance of one or the other photodiode in this second branch depends on the polarization potential: The top photodiode representing the p-Se/electrolyte junction conducts at potentials more *negative* than its photocurrent turn-on potential (ca. 0.20 V) while the bottom one associated with the n-TiO₂/p-Se junction conducts at potentials more *positive* than its corresponding turn-on potential (ca. −0.20 V).

Four (adjustable) parameters are contained in the above equations to simulate the photocurrents and the dark currents respectively, with the "*a*" terms (a_1, a_2, a_1', and a_2') accounting for the stationary current flow (i.e., plateau adjustment) and the "*b*" terms (b_1 and b_2) representing the carrier transit time constants across the two parallel current flow branches in Figure 8. All simulations were performed with MATHCAD 2000 software.

The behavior of pristine TiO₂ (i.e., oxide surface containing no Se islands), in contact with the electrolyte, is simulated in Figure 9a. For this simulation, only the first terms in eqs 1 and 2 were deployed. The values for the simulation parameters are contained in the caption. The resultant simulated profile in
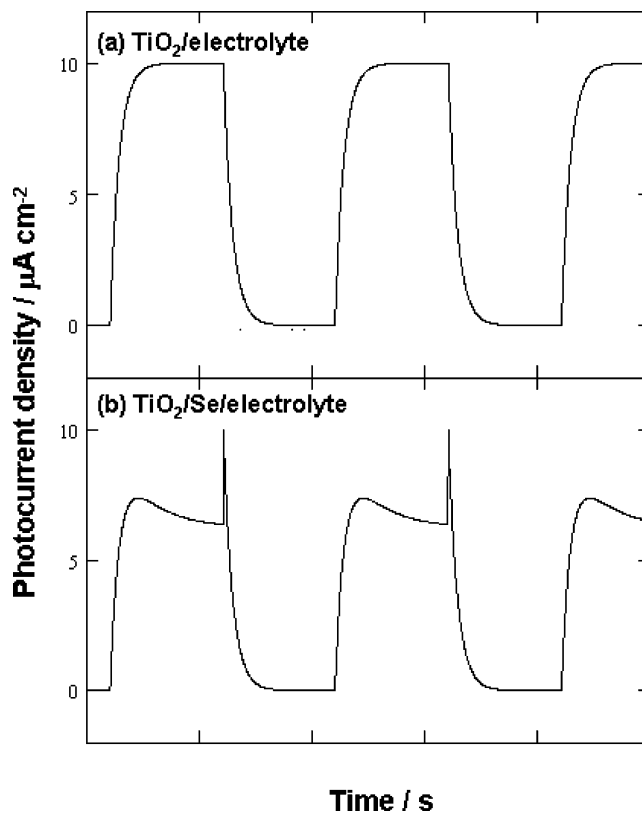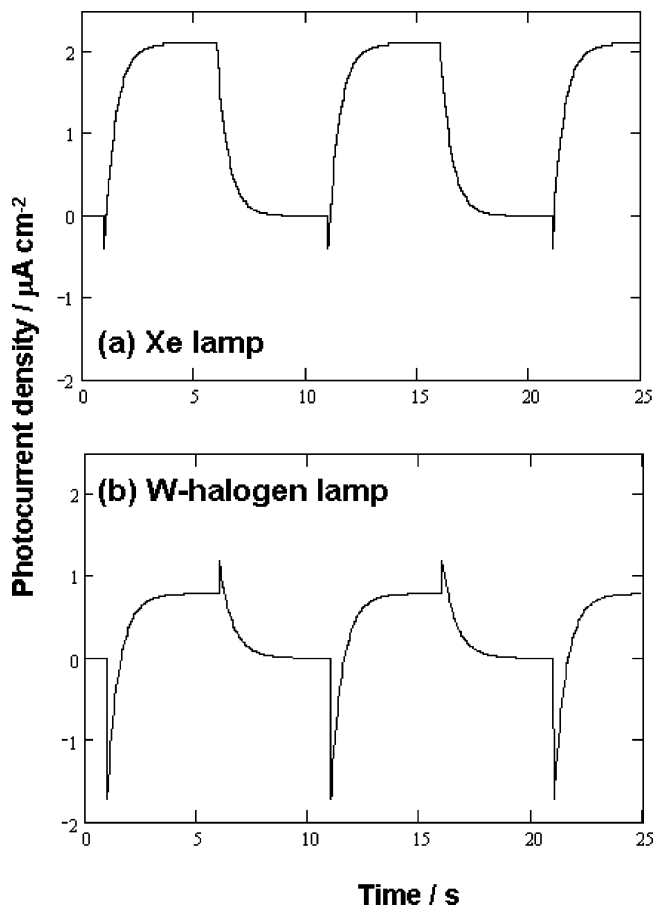

Figure 9. Simulation of the transient photoresponse for pristine TiO₂ (a) and the effect of selenium on the simulated transient photoresponse of TiO₂ (b) with use of eqs 1 and 2. Both cases pertain to Xe arc irradiation. The parameters used were (a) $a_1 = 10\ \mu A\ cm^{-2}$, $b_1 = 2.5\ s^{-1}$, $a_1' = 10\ \mu A\ cm^{-2}$, and (b) $a_1 = 10\ \mu A\ cm^{-2}$, $b_1 = 2.5\ s^{-1}$, $a_2 = 3.4\ \mu A\ cm^{-2}$, $b_2 = 0.7\ s^{-1}$, $a_1' = 10\ \mu A\ cm^{-2}$, $a_2' = 3.4\ \mu A\ cm^{-2}$.

Figure 9a is what would be expected for the photoelectrochemical behavior of an irradiated n-type semiconductor (moderately reverse-biased) in contact with an electrolyte. That is, the photogenerated holes are driven to the electrolyte with consequent generation of an anodic photocurrent. For the simulations in Figure 9b, the contribution of n-TiO₂/p-Se/electrolyte is "turned on", with inclusion of the second terms in eqs 1 and 2.

The effect of the parallel (photodiodes-in-series) branch appears as a slow decrease of the stationary photocurrent ending with a sharp transient at the light "off" point (Figure 9b). The parameter values for the simulations in Figure 9b are again contained in the corresponding caption. The simulated profiles in Figure 9b may be compared with their experimental counterpart in Figure 7 (bottom frame) while the corresponding simulated profile for pristine TiO₂ (Figure 9a) is entirely in accord with experimental data (not shown here). Further, the experimental profile for a reverse-biased case, shown in the top frame of Figure 7, clearly approaches a situation where the current is predominantly driven through the n-TiO₂/electrolyte branch.

Figure 10 simulates the transient photocurrent profiles for the two experimental situations (Figure 6) where the light source was switched from a Xe arc to a W-halogen lamp. Thus Figures 6a and 10a are comparable as are Figures 6b and 10b; the agreement between experiment and model simulation is satisfactory in both cases. The values for the simulation parameters are once again contained in the caption for Figure 10.

For simulating the experimental current−potential profiles in Figure 5, the approach taken was to first consider the photoelectrochemical behavior of the individual n-TiO₂/electrolyte and p-Se/electrolyte components and then combine

Figure 10. Simulation of the transient photocurrent profiles for the two experimental situations shown in Figure 6 where the light source was switched from a Xe arc (a) to a W-halogen lamp (b). The parameters used were (a) $a_1 = 20\ \mu A\ cm^{-2}$, $b_1 = 2.9\ s^{-1}$, $a_2 = 4.0\ \mu A\ cm^{-2}$, $b_2 = 5.0\ s^{-1}$, $a'_1 = 20\ \mu A\ cm^{-2}$, $a'_2 = 0$, and (b) $a_1 = 1.6\ \mu A\ cm^{-2}$, $b_1 = 2.9\ s^{-1}$, $a_2 = 1.4\ \mu A\ cm^{-2}$, $b_2 = 10\ s^{-1}$, $a'_1 = 1.6\ \mu A\ cm^{-2}$, $a'_2 = 0.4\ \mu A\ cm^{-2}$.

them appropriately (see below). While many models are available for simulating the current−potential profiles for semiconductor/electrolytes,[1,18−26] we chose the one by Wilson[21] for its simplicity, transparency, and versatility. Thus the underlying model assumptions are the same as those in the original Wilson treatment (uniform doping level in the semiconductor, carrier recombination confined to the surface, etc.; see refs 21 and 22). The current−potential relationship for each component interface (see above) is computed as follows:

$$i_{TiO_2} = i_{ph}^{TiO_2} + i_d^{TiO_2} \quad (3)$$

$$i_{Se} = i_{ph}^{Se} + i_d^{Se} \quad (4)$$

In eqs 3 and 4, i is the total current, i_{ph} is the photocurrent, and i_d is the dark current and the "TiO$_2$" and "Se" subscripts/superscripts denote the two interfaces, respectively. We utilized the conventional diode expression[2,18,19] for the dark current flow, i.e., exponential dependence of current on potential (see the second terms in the model expressions in the Appendix). The Appendix enumerates the model equations underlying the simulations discussed next. Table 2 contains values for the various parameters for the simulations.

Figure 11 contains simulations of the photocurrent−potential behavior for the individual n-TiO$_2$/electrolyte and p-Se/electrolyte interface components (dashed curves). Also included

TABLE 2: Nominal Values[a] of the Various Simulation Parameters (see eqs A1−A3 in the Appendix)

parameter (units)	value	
	TiO$_2$	Se
α (cm^{-1})	4×10^5	2×10^5
W_0 (cm/V$^{1/2}$)	4×10^{-6}	4×10^{-7}
L (cm)	8×10^{-5}	4×10^{-6}
D (cm^2 s^{-1})	0.025	0.075
k_1 (cm s^{-1})	3×10^{-1}	2×10^{-2}
k_2 (cm s^{-1})	2×10^{-3}	4×10^{-4}
k_d (cm s^{-1})	3×10^{-2}	1×10^{-2}

[a] For some simulations, the values shown were perturbed, see, for example, Figure 12. These perturbations are identified in the corresponding figure captions.
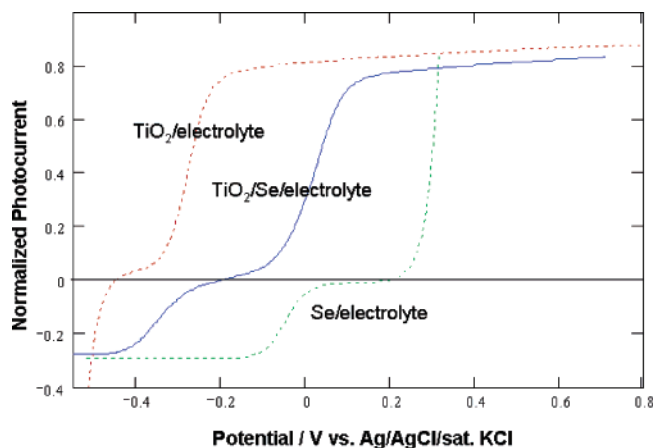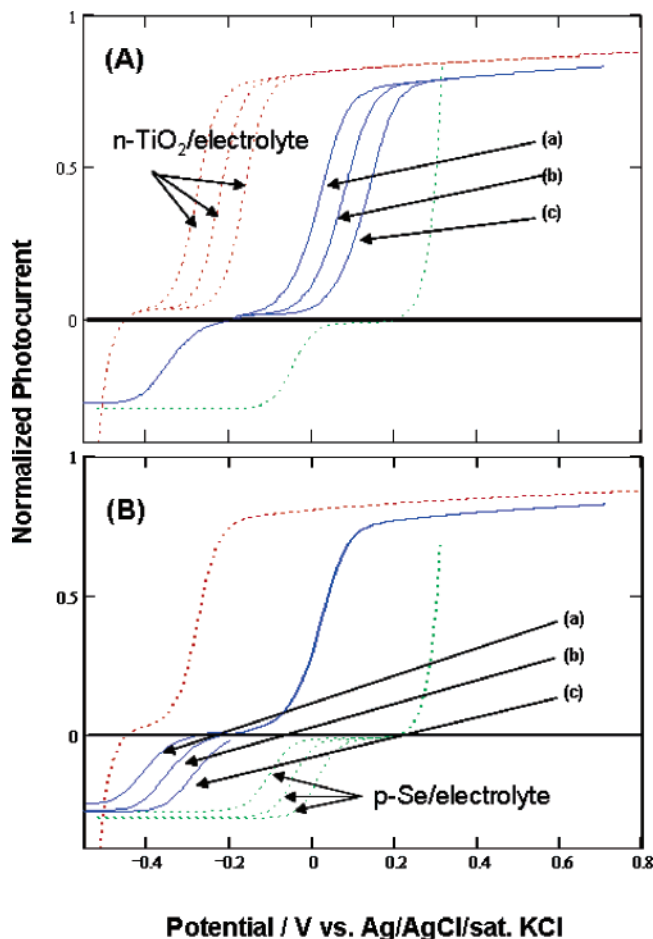

Figure 11. Simulations of the photocurrent−potential behavior for the individual n-TiO$_2$/electrolyte (dashed red line), p-Se/electrolyte (dashed green line), and n-TiO$_2$/p-Se/electrolyte (solid blue line). Parameters are given in Table 2.

in this figure is the composite curve (solid line) for the two photodiodes connected in series back-to-back. The simulation of the n-TiO$_2$/p-Se/electrolyte configuration was performed for the cathodic and anodic branches of the current−potential profile by using four i−V segments that correspond to the dark and irradiated condition of the two semiconductors. Thus, for the cathodic currents, the photocurrent originating from Se and the dark current of TiO$_2$ are combined and the related potentials that satisfy the condition $i_d^{TiO_2} = i_{ph}^{Se}$ were inserted in the equation for i_{ph}^{Se} and plotted as the cathodic photocurrent branch (cathodic solid line). In the same way, in the anodic side, the condition to satisfy is $i_{ph}^{TiO_2} = i_d^{Se}$; again the resulting potentials were used to obtain the combined current response but now for the positive current, i.e., the anodic photocurrent branch (anodic solid line). This equivalence of anodic and cathodic current branches is implicit in considerations of particulate semiconductor suspensions,[27,28] and in fact is a concept inspired by the corrosion community.[29,30]

Recalling that the Wilson model[18,19,21,22] contains an electron-transfer constant, k_1, Figure 12 illustrates the effect of varying this model parameter for n-TiO$_2$/electrolyte (Figure 12A) and p-Se/electrolyte (Figure 12B). The corresponding effect on the composite n-TiO$_2$/p-Se/electrolyte response is also shown in the figure as the solid lines. While the "dark" current branches are unaffected, the variation in k_1 manifests as a shift in the photocurrent branch along the potential axis.

For fitting the above model to experimental data, the parallel current branch attributable to the exposed n-TiO$_2$ regions (Figure 8) must be combined with the composite response obtained from the n-TiO$_2$/p-Se/electrolyte junction. Thus the solid curves in Figures 11 and 12 are in turn combined with the simulated

Figure 12. Simulated effect of varying the electron-transfer constant on the resulting photocurrent−potential curves for TiO$_2$ (A) and Se (B); these are shown as dashed curves. The composite response for the photodiode/electrolyte junction is shown as solid lines. Simulation values for k_1 are the following: (A) $k_1^{Ti} = 3 \times 10^0$ (a), 3×10^{-1} (b), 3×10^{-2} cm s^{-1}(c); (B) $k_1^{Se} = 2.0 \times 10^{-3}$ (a), 2.0×10^{-2} (b), 2.0×10^{-1} cm s^{-1} (c). Other parameters are given in Table 2.

response of the n-TiO$_2$/electrolyte interface to afford the simulated response of the entire assemblage comprised of p-Se islands atop a (contiguous) n-TiO$_2$ surface in contact with the electrolyte. The resulting model simulations are shown as fits (solid lines enveloping the data spikes) to the experimental data (reproduced from Figure 5) in Figure 13. The agreement between experiment and our first-order model is satisfactory. Clearly, the twin-plateau signature in the experimental photocurrent−potential curves (e.g., Figure 5a) is only accommodated by taking into account the exposed n-TiO$_2$/electrolyte regions (i.e., those not covered by p-Se) of the interface. This second plateau in the anodic photoresponse (Figures 5a and 13a) can be viewed as arising from the effect of the reverse-biased n-TiO$_2$ component of the overall n-TiO$_2$/p-Se (photochemical diode)/electrolyte interface.

General Discussion

Considering both the simplicity and first-order nature of our model (see Figure 8), the good agreement between experiment and simulations (cf., Figures 6 and 10, Figures 7 and 9, and Figure 13) is gratifying, and undoubtedly the efficacy of our model is rooted in the compactness of the underlying TiO$_2$ layer (see Figure 1). The lack of an open, microporous network (permeated also by an electrolyte) within the TiO$_2$ phase presumably facilitates the development of space-charge layers at the interfaces with the p-Se regions and with the electrolyte
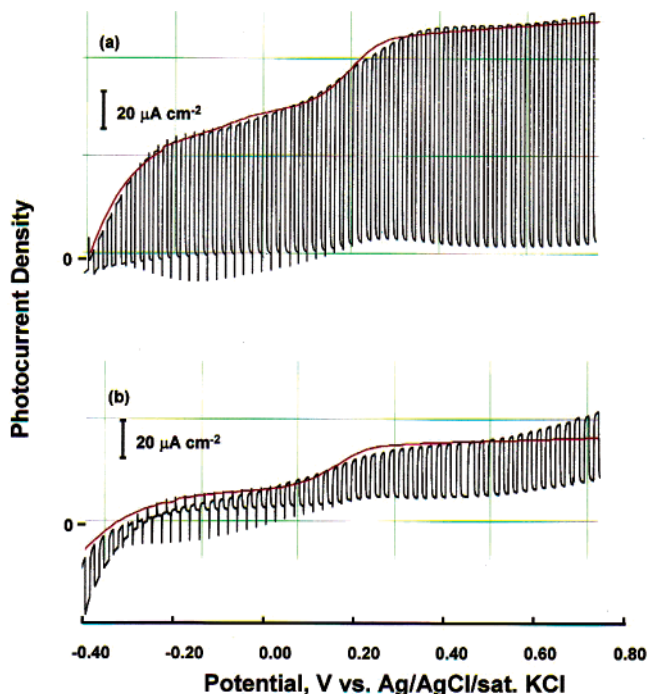
Figure 13. Comparison of the simulated (solid red lines) and the experimental photocurrent−potential curves for n-TiO$_2$/p-Se/electrolyte. The latter are reproduced from Figure 5. The equivalent circuit shown in Figure 8 was used and the parameters are listed in Table 2 for the two photodiodes back-to-back. The parallel current branch for the exposed n-TiO$_2$ regions to the electrolyte uses $S = 1$ (see eq A3).

in regions not covered by Se. The existence of a space charge layer underpins the classical Wilson model albeit for the single crystal case. In our nanostructured film case, these layers probably encompass several TiO$_2$ grains. The close similarity of the voltammogram to that seen for an irradiated *single crystal* semiconductor electrode[18,19] is also indicative of the fact that the bias potential acts across the semiconductor in a not too dissimilar fashion in the two cases.

An additional factor lends further credence to our model. The twin-plateau voltammogram profile that is experimentally observed for the current−potential profiles for the n-TiO$_2$/p-Se/electrolyte interface (Figure 5) shows that the influence of the n-TiO$_2$/electrolyte and n-TiO$_2$/p-Se/electrolyte interfaces in the overall composite photoelectrode system is *additive*. Note that this twin-plateau profile is conspicuously absent for the pristine n-TiO$_2$/electrolyte interface containing no Se islands (Figure 4a).

Concluding Remarks

We have shown how photocatalysis and electrodeposition can be profitably combined to afford novel monolithic composite photoelectrodes comprised of a contiguous and compact TiO$_2$ layer with isolated p-Se regions. These "photochemical diodes" in contact with an inert electrolyte (e.g., Na$_2$SO$_4$) show interesting transient photoresponses whose temporal profiles depend on the wavelength distribution of the excitation light source. A simple equivalent circuit model was used to simulate both the transient photoresponse and the potentiodynamic photoelectrochemical behavior.

11960 *J. Phys. Chem. B, Vol. 109, No. 24, 2005*

de Tacconi et al.

Appendix

The following expressions were used for simulating the current−potential behavior of the individual n-TiO$_2$/electrolyte and p-Se/electrolyte components. The expressions are adapted from the Wilson model, ref 21.

$$i_{TiO_2} = \frac{k_1^{Ti}}{k_1^{Ti} + k_2^{Ti}}\left[1 - e^{-\alpha_{Ti}W_{Ti}} + e^{-\alpha_{Ti}W_{Ti}}\left(\frac{\alpha_{Ti}L_{Ti}}{1 + \alpha_{Ti}L_{Ti}}\right) \times \right.$$
$$\left.\left(\frac{L_{Ti}}{L_{Ti} + \frac{D_{Ti}}{S_{Ti}}}\right)\right] + k_d^{Ti}[1 - e^{-k(V - V_{on}^{Ti})}] \quad (A1)$$

$$i_{Se} = \frac{-k_1^{Se}}{k_1^{Se} + k_2^{Se}}\left[1 - e^{-\alpha_{Se}W_{Se}} + e^{-\alpha_{Se}W_{Se}}\left(\frac{\alpha_{Se}L_{Se}}{1 + \alpha_{Se}L_{Se}}\right) \times \right.$$
$$\left.\left(\frac{L_{Se}}{L_{Se} + \frac{D_{Se}}{S_{Se}}}\right)\right] - k_d^{Se}[1 - e^{-k(V - V_{on}^{Se})}] \quad (A2)$$

In eqs A1 and A2, k_1 and k_2 are the electron transfer and recombination constants (units of cm s^{-1}, ref 21), α is the absorption coefficient (cm^{-1}), W is the depletion layer width [$W = W_0(V - V_{on})^{1/2}$], L is the diffusion length of minority carriers (holes for TiO$_2$ and electrons for Se) in the semiconductor bulk [$L = (D\tau)^{1/2}$, where D is the diffusion coefficient (cm^2 s^{-1}) and τ is the transit time (s)], k_d is the dark current constant, $k = q/kT = 38.65$ V^{-1} (where q is the electronic charge, k is the Boltzmann constant, and T is the absolute temperature), and V_{on} is the photocurrent "turn-on" potential, a parameter whose value is close to the flat-band potential. In each of the expressions, S is a boundary-condition parameter given by:[21]

$$S = (k_1 + k_2)e^{k(V - V_{on})} - $$
$$\frac{D(1 - e^{-\alpha W})}{Le^{-\alpha W}\left(\frac{\alpha L}{\alpha L + 1}\right)}\left[1 + \frac{(1 - e^{-\alpha W})}{e^{-\alpha W}\left[\frac{\alpha L}{\alpha L + 1}\right]}\right]^{-1} \quad (A3)$$

Values for the various parameters that were used for the simulations in Figures 12−14 are contained in Table 2. Values of the "turn-on" potential for TiO$_2$ and Se were taken as −0.45 and 0.20 V; these were obtained from experimental data as in Figure 4.

References and Notes

(1) Nozik, A. J.; Memming, R. *J. Phys. Chem.* **1996**, *100*, 13061.
(2) Rhoderick, E. H. *Metal-Semiconductor Contacts*; Clarendon Press: Oxford, UK, 1980.
(3) Nozik, A. J. *Appl. Phys. Lett.* **1977**, *30*, 567.
(4) Rajeshwar, K.; de Tacconi, N. R.; Chenthamarakshan, C. R. *Chem. Mater.* **2001**, *13*, 2765.
(5) Khaselev, O.; Turner, J. A. *Science* **1998**, *280*, 425.
(6) Chenthamarakshan, C. R.; Ming, Y.; Rajeshwar, K. *Chem. Mater.* **2000**, *12*, 3538.
(7) Somasundaram, S.; Chenthamarakshan, C. R.; de Tacconi, N. R.; Ming, Y.; Rajeshwar, K. *Chem. Mater.* **2004**, *16*, 3846.
(8) Tan, T. T. Y.; Zaw, M.; Beydoun, D.; Amal, R. *J. Nanopart. Res.* **2002**, *4*, 541.
(9) Natarajan, C.; Nogami, G. *J. Electrochem. Soc.* **1996**, *143*, 1547.
(10) Shen, P. K.; Syed-Bokhari, J.; Tseung, A. C. C. *J. Electrochem. Soc.* **1991**, *138*, 2778.
(11) Switzer, J. A. *Am. Ceram. Bull.* **1987**, *66*, 1521.
(12) Karuppuchamy, S.; Nonomura, K.; Yoshida, T.; Sugiura, T.; Minoura, H. *Solid State Ionics* **2002**, *151*, 19.
(13) Han, L. M.; Rajeshwar, K.; Timmons, R. B. *Langmuir* **1997**, *13*, 5941.
(14) Wagner, C. D.; Riggs, W. M.; Davis, L. E.; Mulder, J. F.; Mattenberg, G. E. *Handbook of X-Ray Photoelectron Spectroscopy*; Perkin-Elmer Corp. (Physical Electronics Division): Eden Prairie, MN, 1979.
(15) Rajeshwar, K.; Singh, P.; DuBow, J. *Electrochim. Acta* **1978**, *23*, 1117.
(16) Rao, M. V.; Rajeshwar, K.; Pai Verneker, V. R.; DuBow, J. *J. Phys. Chem.* **1980**, *84*, 1987.
(17) Frese, K. W., Jr. *J. Appl. Phys.* **1982**, *53*, 1571.
(18) Rajeshwar, K. In *Electron Transfer in Chemistry*; Balzani, V., Ed.; Wiley-VCH: Weinheim, Germany, 2001; Vol. 4, p 279.
(19) Rajeshwar, K. In *Encyclopedia of Electrochemistry*: *Semiconductor Electrodes and Photoelectrochemistry*; Licht, S., Ed.; Wiley-VCH: Weinheim, Germany, 2002; Vol. 6, p 1.
(20) Butler, M. A. *J. Appl. Phys.* **1977**, *48*, 1914.
(21) Wilson, R. H. *J. Appl. Phys.* **1977**, *48*, 4292.
(22) Wilson, R. H. *CRC Crit. Rev. Solid State Mater. Sci.* **1980**, *10*, 1.
(23) Reichman, J. *Appl. Phys. Lett.* **1980**, *36*, 574.
(24) Reiss, H. *J. Electrochem. Soc.* **1978**, *125*, 937.
(25) Fonash, S. J. *Solar Cell Device Physics*; Academic Press: San Diego, CA, 1981.
(26) Hammett, A. In *Comprehensive Chemical Kinetics*; Compton, R. G., Hancock, G., Eds.; Elsevier: Amsterdam, The Netherlands, 1999; pp 223−280. See also references therein.
(27) Miller, D. S.; Bard, A. J.; McLendon, G.; Ferguson, J. *J. Am. Chem. Soc.* **1981**, *103*, 5336.
(28) Rajeshwar, K.; Ibanez, J. G. *J. Chem. Educ.* **1995**, *72*, 1044.
(29) Wagner, C.; Traud, W. *Z. Elektrochem.* **1938**, *44*, 391.
(30) Steigerwald, R. F. *Corrosion* **1968**, *24*, 1.